IOP Publishing | Bureau International des Poids et Mesures Metrologia

Metrologia **51** (2014) 174–182 doi:10.1088/0026-1394/51/3/174

First accuracy evaluation of NIST-F2

Thomas P Heavner[1], Elizabeth A Donley[1], Filippo Levi[2], Giovanni Costanzo[3], Thomas E Parker[1], Jon H Shirley[1], Neil Ashby[1], Stephan Barlow[1] and S R Jefferts[1]

[1] Time and Frequency Division, National Institute of Standards and Technology, Boulder, CO 80305, USA
[2] Istituto Nazionale di Ricerca Metrologica, INRIM, Strada delle Cacce 91, 10135 Torino, Italy
[3] Politecnico di Torino, C. Duca degli Abruzzi 24 10129 Torino, Italy

E-mail: heavner@boulder.nist.gov

Received 23 October 2013, revised 13 March 2014
Accepted for publication 17 March 2014
Published 1 May 2014

Abstract

We report the first accuracy evaluation of NIST-F2, a second-generation laser-cooled caesium fountain primary standard developed at the National Institute of Standards and Technology (NIST) with a cryogenic (liquid nitrogen) microwave cavity and flight region. The 80 K atom interrogation environment reduces the uncertainty due to the blackbody radiation shift by more than a factor of 50. Also, the Ramsey microwave cavity exhibits a high quality factor (>50 000) at this low temperature, resulting in a reduced distributed cavity phase shift. NIST-F2 has undergone many tests and improvements since we first began operation in 2008. In the last few years NIST-F2 has been compared against a NIST maser time scale and NIST-F1 (the US primary frequency standard) as part of in-house accuracy evaluations. We report the results of nine in-house comparisons since 2010 with a focus on the most recent accuracy evaluation. This paper discusses the design of the physics package, the laser and optics systems and the accuracy evaluation methods. The type B fractional uncertainty of NIST-F2 is shown to be 0.11×10^{-15} and is dominated by microwave amplitude dependent effects. The most recent evaluation (August 2013) had a statistical (type A) fractional uncertainty of 0.44×10^{-15}.

Keywords: atomic clock, frequency standard, SI second, caesium

(Some figures may appear in colour only in the online journal)

1. Introduction

The Time and Frequency Division of the National Institute of Standards and Technology (NIST) in Boulder, CO has operated NIST-F1, a laser-cooled caesium (Cs) fountain primary frequency standard, since 1998 [1, 2]. Currently, the type B fractional uncertainty in NIST-F1 is 0.31×10^{-15} and is dominated by the uncertainty in the blackbody radiation (BBR) shift correction, which is 0.28×10^{-15} (this corresponds to a 1 degree uncertainty in the radiation environment as seen by the atoms in NIST-F1). To improve the performance of the NIST primary frequency standard, we sought to reduce the uncertainty due to the BBR effect. To accomplish this goal and to better understand the accepted model of the BBR shift, we developed NIST-F2, a laser-cooled Cs fountain primary frequency standard in which the microwave cavity structure and flight tube operate at cryogenic temperatures (80 K).

Many national standards laboratories operate Cs fountain primary frequency standards that contribute to International Atomic Time (TAI). Current information regarding primary frequency standards can be obtained through the Bureau International des Poids et Mesures (BIPM) [3]. The performance of Cs fountains has improved steadily since their introduction [4], and several groups now report type B fractional uncertainties in the range of 2×10^{-16} to 3×10^{-16} [5–8].

NIST-F1 operates nominally at room temperature and has a fractional BBR bias of -21.85×10^{-15} whereas the BBR bias in NIST-F2 is less than 1×10^{-16}. This allows for a direct measurement of the effect in NIST-F1 by use of NIST-F2. Operation of a fountain at cryogenic temperatures has additional advantages as well as challenges due to the high quality factor (Q) of the 80 K Ramsey microwave cavity. The Q is significantly higher due to the increase in conductivity of copper at cryogenic temperatures which reduces the distributed cavity phase shift (DCPS), a significant source of uncertainty in many Cs primary frequency standards. On the negative side, the high Q creates a concern regarding cavity pulling bias

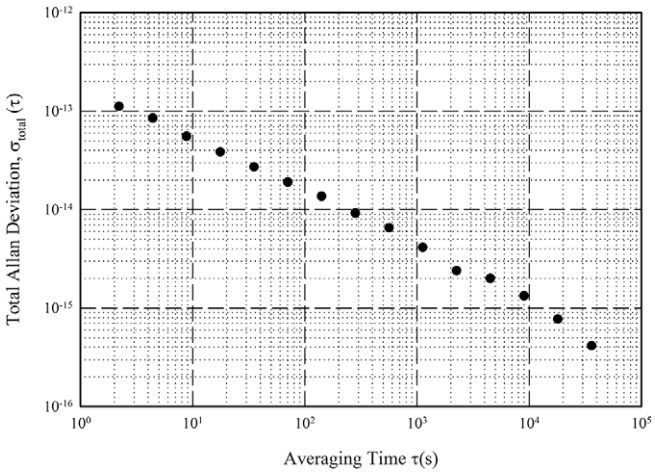

Figure 1. The Total deviation (TOTDEV) of NIST-F2 operating at high atomic density where the stability is $\approx 1.7 \times 10^{-13}\tau^{-1/2}$. The detected atom number is, approximately, 2×10^4. The measurement was made using a commercial hydrogen maser as a reference.

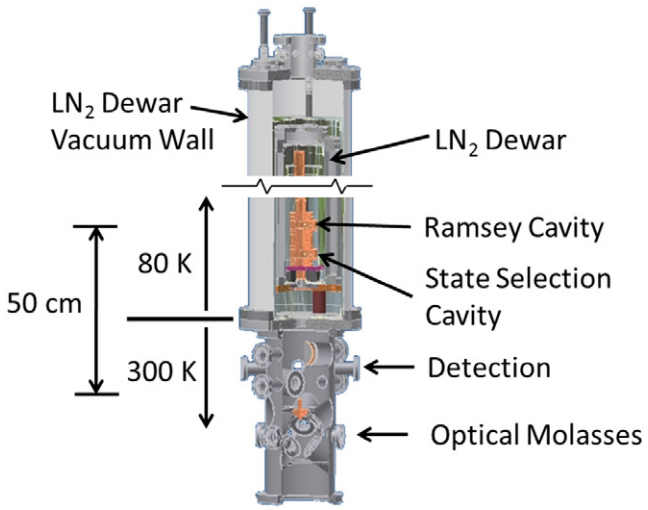

Figure 2. A sectional view of the NIST-F2 physics package. The laser-cooled Cs source chamber operates in the (1,1,1) geometry. Directly above the source region and within the same vacuum chamber is the two-level detection zone. A short bellows with a thermal break (not shown here) connects the lower half of the system to the cryogenic microwave cavity structure. The cavity structure resides on a cold plate that is in thermal contact with the LN_2 dewar. The C-field and three layers of magnetic shields are located within the vacuum section of the LN_2 dewar. For clarity, the entire dewar structure is not shown above, but it extends approximately 1.5 m above the source/detection chamber.

if the cavity resonance is not sufficiently close to the atomic resonance.

The design concepts for NIST-F2 were first presented in 2003 [9] and in some more detail in 2005 [10]. Two identical physics packages were constructed and assembled at NIST in Boulder, CO. One resides at NIST and the second was delivered to the Istituto Nazionale di Ricerca Metrologica (INRIM) in Torino, Italy [11]. Clock transitions and preliminary results were first presented in 2008 [8]. In the last several years, we have worked on improving the stability and characterizing the accuracy of NIST-F2. Figure 1 shows the Allan deviation of NIST-F2 operating at high atom number, illustrating a stability of $\approx 1.7 \times 10^{-13}\tau^{-1/2}$.

Here we present measurements from September 2010 to August 2013. Many systematic biases are evaluated repeatedly in NIST-F2 (as well as NIST-F1), so the type B uncertainties vary during this period. For example, the microwave power shift reported in this paper is from measurements in November 2012. However, since the microwave synthesizer was slightly modified in 2013, it was necessary to re-evaluate the bias due to microwave amplitude effects. The final uncertainties for the August 2013 evaluation (which was submitted to the BIPM for inclusion into *Circular-T*) are slightly larger due to the shorter amount of time measuring the biases.

The NIST-F2 apparatus is described in section 2 of this paper. The evaluation procedures and systematic biases are outlined in section 3. Section 4 presents the results of the accuracy evaluations of NIST-F2, which are performed using the NIST maser-based time scale and NIST-F1 as references.

2. NIST-F2 apparatus

2.1. Physics package

The design, operating principles and preliminary results from NIST-F2 have been discussed in previous publications [9, 10, 12]. The physics package, shown in figure 2, consists of a combined cold atom source and detection chamber which is attached to a copper microwave cavity structure within a liquid nitrogen (LN_2) dewar.

The cooling/detection chamber has six windows in the (1, 1, 1) configuration for cooling and launching atoms. Additional ports and windows in the mid-plane provide access for the repump laser, cameras and caesium ovens. The detection region has two (upper and lower) zones with identical geometry. Each has a half-spherical mirror within the vacuum chamber for light collection. The mirror faces a re-entrant window against which a detector module is located. The detector module contains light collecting optics, a photodiode and an amplifier. The composite chamber design minimizes the distance between the atom cooling region and the microwave interrogation region.

Above the source/detection chamber is a LN_2 dewar within an insulating vacuum chamber. The copper microwave cavity and flight tube structure are mounted on a cold plate that in turn is attached to the LN_2 dewar. A solenoid which generates the C-field (the C-field is the magnetic field used to provide a quantization axis) and three layers of magnetic shields reside within the LN_2 dewar vacuum chamber.

The top flange of the LN_2 dewar houses feedthroughs for microwave signals, temperature sensors, LN_2 fill lines, wiring for the C-field, coils to generate transverse magnetic fields, shim coils and the magnetic shield degauss system.

The state-selection and Ramsey microwave cavities are essentially identical to the NIST-F1 cavities [2, 13] except that they are designed to be resonant at LN_2 temperatures. The cavities have four, strongly undercoupled, mid-plane feeds to minimize DCPSs.

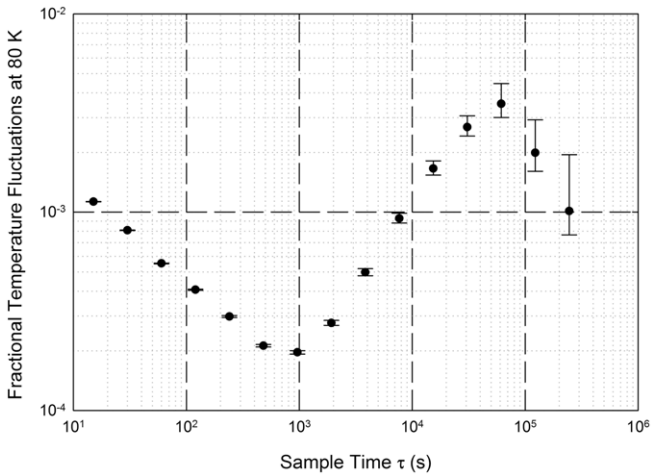

Figure 3. A plot of the Allan deviation of fractional temperature fluctuations of the Ramsey microwave cavity (80 K) illustrating the long-term temperature stability.

The LN_2 level in the dewar is controlled by an automatic system. Because the Ramsey cavity is not exactly on resonance at the nominal temperature provided by the LN_2 dewar, it is necessary to pump on the volume above the LN_2, thus lowering the temperature of the LN_2 bath, to bring the cavity into resonance. The long-term temperature of the Ramsey cavity structure is controlled by a programmable servo system that monitors the pressure above the LN_2 temperature and opens and closes a valve to a pump to stabilize the pressure. This valve is typically open with a duty cycle >90% and a time constant of many hours. The valve, pump and associated manifold hardware are located several metres away from NIST-F2 and are vibrationally isolated from the physics package. Operation of NIST-F2 is paused during a LN_2 fill sequence which occurs every ≈10 h and lasts for a few minutes. Figure 3 shows the Allan deviation of the temperature of the Ramsey cavity over 14 days.

While many of the NIST-F2 parameters are varied in the accuracy evaluation process, typically the optical molasses load time is ≈0.2 s and the atom ball has a temperature of 0.46 μK and a characteristic size of ≈3 cm (FWHM). The standard Ramsey time is ≈0.6 s and the C-field is ≈2.5 mG (250 nT).

2.2. Laser and optics

The laser system for NIST-F2 is based on a commercial titanium sapphire ring laser pumped by a high-power diode system operating at 532 nm. This provides about 1 W of 852 nm of light with a linewidth of 50 kHz. This light is delivered via a polarization maintaining (PM) optical fibre cable to a network of six double-pass acousto-optic modulator (AOM) assemblies, which generate the six independent cooling and launching beams [14]. The output beam of each individual AOM assembly is injected into a PM fibre, which travels to the physics package. Six output collimators are attached to the vacuum chamber at the re-entrant windows at the source region. Each output collimator has a beam pick off that directs a small amount of light onto a photo-detector. The six photo-detector signals from the collimators are used in a servo control system whereby the light levels during molasses, launch, post-cool, are controlled by adjusting the RF power delivered to each corresponding AOM.

2.3. Microwave synthesis

NIST-F2 uses the same microwave synthesis architecture as NIST-F1 [1, 15]. A high-performance quartz oscillator is locked (≈10 s time constant) to a reference signal from a hydrogen maser in the NIST time scale. This signal is used to make 100 MHz using a multiplier chain which in turn is used to phase-lock a dielectric resonator oscillator (DRO) that produces 9.200 GHz. A single-sideband mixer is used with a computer-controlled synthesizer signal at 7.368 MHz to make 9.193 GHz to drive clock transitions. This system has been described in detail in previous work and exhibits a noise floor below the quantum projection noise level in NIST-F2 at the normally used atom number [1].

2.4. NIST maser time scale

A NIST hydrogen maser-based time scale serves as a flywheel reference during the long evaluation intervals of NIST-F2 (and NIST-F1). The effective use of this time scale and deadtime issues are discussed in [16]. Additionally, if both fountains are running simultaneously, we are able to use the long-term stability of NIST-F1 as a reference for NIST-F2, thus eliminating the time scale entirely.

3. NIST-F2 systematic biases

3.1. Relativistic effects

The gravitational redshift in Boulder, CO is a large systematic frequency bias for both NIST-F1 and NIST-F2. This bias has been well studied for NIST-F1 [17], and because NIST-F2 is located in an adjacent laboratory on the same floor as NIST-F1, we can easily correct for this bias. Since this is a relativistic effect, our correction here includes the second-order Doppler effect contribution. The total fractional correction due to relativity (gravitational redshift and second-order Doppler) for NIST-F2 is $(+179.87 \pm 0.03) \times 10^{-15}$.

3.2. Second-order Zeeman shift

We use a similar method as with NIST-F1 [2] to measure the second-order Zeeman shift. First, the magnetic field along the flight tube is mapped by launching the atoms to various apogees, typically in 1 cm increments. A rectangular coil extending the length of the flight tube is used to generate a magnetic field transverse to the C-field. In field mapping mode, a low frequency (≈1 kHz) transverse magnetic field is turned on for 100 ms at apogee to drive the $|3, 0\rangle \rightarrow |3, 1\rangle$ transition. This process generates a map of the magnetic field along the vertical axis of the flight tube. The map is then integrated with respect to the ballistic trajectory of the atom cloud to predict the central fringe on the $|3, 1\rangle \rightarrow |4, 1\rangle$ magnetic field-sensitive manifold as a function of launch height. This prediction is then

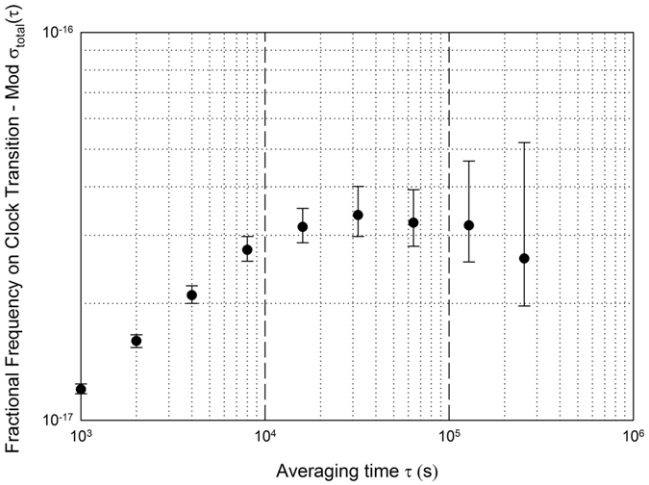

Figure 4. The total deviation of the frequency fluctuations on the clock transition in NIST-F2 caused by fluctuations in the magnetic field. These data are obtained by measurements of the $|3, 1\rangle \rightarrow |4, 1\rangle$ transition in NIST-F2, which are then translated into frequency shifts on the clock transition.

compared with measurements of the $|3, 1\rangle \rightarrow |4, 1\rangle$ Ramsey fringes for various launch heights. Using this method we are able to unambiguously identify the central field sensitive fringe.

In NIST-F2 we have concerns about the adequacy of magnetic shielding and the possibility of losing identity of this central fringe during long evaluation campaigns. So, we also measure magnetic field transitions approximately every 10^3 s during standard operation. To achieve this, we employ a two-stage magnetic field line servo. First, by use of the same magnetic field coil along the flight tube as described above, a low frequency field transverse to the C-field axis excites the $|3, 0\rangle \rightarrow |3, 1\rangle$ transition not only at apogee but continuously during the trajectory of the atoms [18]. The resonance is measured by use of a square wave servo (the same method used to measure the clock transition). This provides a measurement of the average magnetic field as seen by the atoms during their trajectory. While this measurement does not allow for an adequately accurate second-order Zeeman correction, it does provide enough precision to generate an unambiguous initial estimate for the control software to find and lock on the central fringe on the $|3, 1\rangle \rightarrow |4, 1\rangle$ manifold. This is the second stage of the magnetic field measurement servo. Thus, we have a good record of small magnetic field fluctuations in the time domain and are able to apply the second-order Zeeman correction in near real-time. Figure 4 is the Allan deviation of magnetic field measurements over a six day interval during standard NIST-F2 operation.

We assign an uncertainty in the measurement of the $|3, 1\rangle \rightarrow |4, 1\rangle$ central fringe of ± 0.07 Hz (≈ 10 pT), which corresponds to a fractional uncertainty of 0.02×10^{-15} in the second-order Zeeman correction. This uncertainty is determined from an analysis of the servo behaviour when using an initial estimate generated by the first-stage of the field servo that may miss at the one-tenth of a fringe level coupled with a small number of measurements. The measurements occur approximately every 20 min and last for about 10 s. If necessary, this uncertainty can be reduced in the future through optimization of the servo settings or by increasing the magnetic field servo duty cycle.

The NIST-F2 field map is also used to estimate any bias due to magnetic field inhomogeneity. The theory in [19] is used to predict the fractional frequency bias which is found to be $< 1 \times 10^{-17}$.

3.3. Spin-exchange shift

The spin-exchange shift is evaluated by operating NIST-F2 over a range of atomic densities while using the NIST maser timescale or NIST-F1 as a local oscillator reference. Variations in the atomic density are achieved by making changes to the molasses load time and/or Cs oven temperature. Measurements show no change in the atomic cloud parameters (radius, height, temperature or position) at the 5% level within the range of the parameters used in NIST-F2. We use the same procedure for determining the spin-exchange bias as used for NIST-F1, the details of that spin-exchange extrapolation process and the resulting uncertainties are described in detail in [16] and are not repeated here. The resulting bias is mostly a type A uncertainty, but it includes a small type B uncertainty for completeness. The bias shown is only for one atomic density, the low density, where the majority of the time during an evaluation is spent. Typical cycle time between various atomic densities is one or more days. The low density condition in NIST-F2 corresponds to about 7500 detected atoms.

There is no single spin-exchange shift correction since NIST-F2 operates over a range of atomic densities. The type B aspect of the shift in NIST-F2 is surprisingly small due to the operation at an atom temperature of 0.46 µK. This corresponds to the maximum in the spin-exchange shift versus temperature curve, an unfortunate place to operate but one with no linear change in the spin-exchange coefficient with variations in temperature [20]. This, along with the lack of change in the atomic cloud parameters with changes in atom number, makes the type B uncertainty quite small.

A typical fractional frequency shift in NIST-F2 operating at low density due to the spin-exchange bias is $(-0.71 \pm 0.24) \times 10^{-15}$ with the uncertainty being the result of a month long measurement. Non-linear effects are included as type B with an uncertainty of 0.02×10^{-15}.

3.4. Blackbody radiation (BBR) shift

Since the Cs clock transition is evaluated in a cryogenic microwave cavity and flight tube (approximately 80 K) the total BBR fractional bias in NIST-F2 is $< 10^{-16}$.

The temperature of the NIST-F2 microwave cavity and flight tube structure is measured using platinum resistance temperature detectors (RTDs) at several locations along the length. The RTDs show a temperature gradient between the Ramsey cavity and the apogee of the Cs atoms of ≈ 1 K. A small amount of room temperature (300 K) radiation enters the flight tube through the apertures that allow the cold atoms to enter the Ramsey interrogation structure. However, a light baffle between the room-temperature source chamber and the cryogenic microwave cavities reduces the amount of room

temperature radiation that scatters up the flight tube. The opening of this entrance tube is a source of room temperature photons into the cryogenic Ramsey interrogation region of the frequency standard. The entrance tube, state-selection cavity, Ramsey cavity, and the drift region are all nominally at 80 K. The lower 8 cm of the copper tubing is threaded to prevent high-angle room-temperature reflected optical photons from entering the Ramsey interrogation region. The state selection cavity provides further light trapping of these high-angle room temperature optical photons, thus a 1 cm diameter disc of 291 K radiation therefore enters the bottom end of the region and the rest of the walls are nominally at 80 K. We model the effect of this disc of high-temperature photons along with the temperature gradient in the cryogenic structure to find an effective temperature, $T_{\rm eff}$, as experienced by the atoms along the ballistic trajectory to estimate the BBR shift in NIST-F2. This procedure is described in more detail in [21].

The BBR fractional shift in Cs is given by

$$\frac{\Delta\omega}{\omega_0} = \beta\left(\frac{T_{\rm eff}}{300\,{\rm K}}\right)^4\left[1+\varepsilon\left(\frac{T_{\rm eff}}{300\,{\rm K}}\right)^2\right]. \qquad (1)$$

Using the values of $\beta = (-1.710 \pm 0.006) \times 10^{-14}$ [22] and $\varepsilon = 0.013 \pm 0.001$ [23] we determine the fractional blackbody shift for NIST-F2 to be $(-0.087 \pm 0.005) \times 10^{-15}$. Measurements of NIST-F2 compared against NIST-F1 provide an independent measurement of these BBR coefficients [21]. The uncertainty in $T_{\rm eff}$ is ± 1 K with a corresponding uncertainty in the BBR frequency shift of $\frac{\Delta\omega}{\omega_0} < 5 \times 10^{-18}$.

3.5. Microwave effects

Effects that are known to have microwave power dependent biases include spurious terms in the microwave field [24], microwave leakage [25], DCPSs [26, 27] and the microwave lensing effect [28, 29]. Unfortunately it is essentially impossible to cleanly separate all of the above effects by a simple sequence of measurements. We therefore discuss each of these effects separately and then finally discuss the overall microwave effects in the error budget of the standard.

3.5.1. Distributed cavity phase shift. Early studies of TE_{011} cavities as used in Cs fountains focused on phase variations due to power flow, but presented no rigorous investigations of the effect of the phase variations on the Cs clock transition [30, 31]. The power dependence of frequency shifts due to cavity phase variations was first modelled by our group in [27]. Here a two-level system including cavity phase variations was solved yielding Ramsey line shape distortions as a function of microwave amplitude. The groups at Penn State and Observatoire de Paris later extended the analysis in [32, 33] resulting in useful methods to measure the DCPS by tilting the microwave cavity with respect to gravity and driving the clock transition using opposing feeds. This has led to a significant improvement in the understanding of the DCPS in fountain standards.

Using the notation in [33] we can analyse the frequency shift induced by the various normal modes. In NIST-F2, the

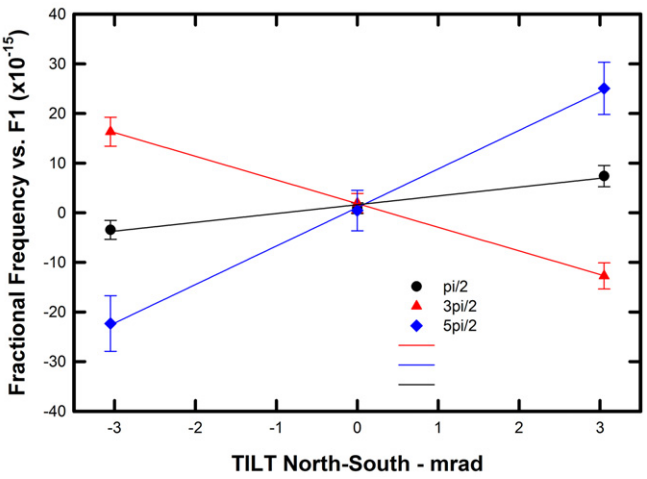

Figure 5. The measured frequency bias measured in NIST-F2 as a function of vertical tilt and microwave power. Here microwaves are introduced from alternate feeds to maximize the DCPS effect. NIST-F2 is tilted in two orthogonal directions, one shown here as North–South and the other as East–West, which give very similar results. These measured tilt sensitivities are used to confirm the fountain verticality and estimate $m = 1$ DCPS bias uncertainties.

measured cavity Q is quite high ($Q = 53\,500$), equal to the calculated Q, and the cavity is basically unloaded (insertion loss ≈55 dB). The Q of the essentially identical NIST-F1 cavity operating at 300 K is 22 500 and this difference is due to the higher electrical conductivity in copper at 80 K versus 300 K.

The $m = 0$ DCPS, which is essentially a longitudinal phase shift, has an amplitude considerably less than $\delta f/f < 1 \times 10^{-18}$ under normal operational conditions. The two orthogonal $m = 1$ modes are excited in superposition in the NIST-F2 cavity due to the geometry of the four feeds. Because the loaded (measured) cavity Q is essentially that predicted by theory, we can largely exclude shifts due to inhomogeneous wall resistivity, or imbalances due to feed coupling. Cavity feeds are balanced in both phase ($\delta\varphi \leqslant 75$ μrad) and amplitude ($\delta b/b \leqslant -60$ dB (10^{-3})) using the measured atomic responses (transition probabilities). Because the cavity is strongly undercoupled, the feeds do not interact with each other, it is therefore unnecessary to balance the feeds as described in [33]. Further, the detection system has been carefully designed to minimize vignetting with overall detection efficiency across the atomic sample being uniform at the 10% level.

The measured tilt sensitivity of the NIST-F2 cavity when driving one microwave feed versus the opposite feed indicates the fountain verticality to be within 100 μrad, consistent with both the design verticality of 100 μrad and the mechanically (spirit-level) measured verticality of the device of 20 μrad (the agreement between the various methods of measuring verticality is comforting, but the 100 μrad uncertainty is used in the analysis). Figure 5 shows the results of measurements taken at various tilt angles along one axis and at various microwave power levels. Note that measurements were made as the fountain was tilted with respect to two orthogonal axes (North–South, shown, and East–West) and the results decomposed into tilt sensitivities for the two $m = 1$ modes. The resulting $m = 1$ tilt sensitivities predict no frequency shift with an uncertainty

Table 1. The systematic biases considered for NIST-F2. Units are fractional frequency $\times 10^{-15}$. The second-order Zeeman bias is measured at regular intervals during the operation of NIST-F2. Consequently, there is no fixed value for this bias and the result here is typical. Similarly, NIST-F2 operates at a variety of atomic densities, so there is no fixed spin-exchange bias. The value given here is the spin-exchange bias at low density. These uncertainties are typical of a 30 day evaluation.

Physical effect	Magnitude	Uncertainty
Gravitational redshift	+179.87	0.03
Second-order Zeeman	+286.06	0.02
Blackbody radiation	−0.087	0.005
Spin-exchange (low density)	(−0.71)[a]	(0.24)[a]
Spin-exchange non-linearity	0	0.02
Microwave amplitude effects		
Distributed cavity phase shift (DCPS)		
$m = 0$	<0.01	<0.01
$m = 1$	0	0.028
$m = 2$	0	0.02
Microwave power	<0.01	0.08
Microwave spurious	0	0.05
Cavity pulling	0.015	0.015
Rabi pulling	<0.01	<0.01
Ramsey pulling	<0.01	<0.01
Majorana transitions	<0.01	<0.01
Fluorescence light shift	<0.01	<0.01
Dc Stark effect	<0.01	<0.01
Background gas collisions	<0.01	<0.01
Bloch–Siegert	<0.01	<0.01
Integrator offset	<0.01	<0.01
Total type B Standard uncertainty		0.11

[a] For information purposes only. Not used in the total. See section 3.3 and [16] for details.

of $\delta f/f = 2 \times 10^{-17}$ for each mode. We have also measured the tilt sensitivity over the same 6.2 mrad range with both feeds driven. This also results in no measureable fractional frequency shift with an uncertainty of $\delta f/f = 2 \times 10^{-17}$ for a 100 µrad tilt. Unlike the typical case for a two-feed cavity, the $m = 2$ mode is essentially unexcited in this cavity, and the frequency shift associated with $m = 2$ is therefore suppressed, with the result that the predicted $m = 2$ DCPS is $\delta f/f \leqslant 2 \times 10^{-17}$. These results are summarized in the uncertainty budget shown in table 1.

3.5.2. Microwave leakage. Microwave leakage can occur in two distinct ways in a state-selected atomic fountain; either between the two Ramsey pulses (e.g. above the microwave cavity), or after the second Ramsey pulse (below the microwave cavity) [25]. In NIST-F2 the drift tube above the microwave cavity is a circular waveguide that is shorted at the upper end. The length is carefully chosen to be anti-resonant at the 9.193 GHz clock transition frequency, and the only propagating mode is a TE_{11} mode, which should not be excited by the cavity mode and in any case should cause no frequency shift to first-order. This leaves the possibility of leakage below the microwave cavity, which has a characteristic signature with microwave amplitude of maximizing (with alternating sign) at odd $\pi/2$ excitation levels and generally scaling with excitation level. The test for this behaviour is discussed below.

3.5.3. Microwave spurious spectrum effects. We have measured the spectrum of the synthesizer, which is generally very similar to that described in [15], and, along with the theory presented in [24] conclude that any frequency bias caused by the microwave spectrum is smaller than $\delta f/f = (0 \pm 0.05) \times 10^{-15}$. This does not include effects of pulsed operation as discussed in [24] and as measured using the apparatus described in [34]. We have looked for pulsed effects by varying the cycle and Ramsey time and seen no evidence; further investigation will be made using an apparatus as described in [34].

3.5.4. Microwave lensing. This shift was first discussed in [28] and the results of that and subsequent work [5] have been applied by several primary standards groups to correct for this bias. The theory presented in [28] contains errors. For example, the magnetic field defining equation ($B(r) = \cos(k_{1x}x)\cos(k_{1z}z)$) has no units and no amplitude factor. Most importantly, equations (5) and (6) of [28] predict a frequency shift in the limit of zero microwave excitation. All systematic biases should be completely understood before applying corrections to a standard. Therefore, we have spent considerable time and effort independently developing a theoretical model of the microwave lensing bias [29]. In this work, we have significantly extended and corrected the ideas presented in [28] including a full treatment of the atomic wave packet behaviour. In NIST-F2, under normal operating conditions, any microwave lensing shift scales just like the microwave leakage shift and is therefore treated below.

3.5.5. Generalized power dependence. As discussed above, we measure the frequency shift of NIST-F2 as a function of microwave amplitude to look for this family of frequency biases, which depend on the microwave field amplitude. The first-order behaviour for many of the effects can be approximated by

$$\frac{\delta f}{f} = A n \sin\left(\frac{n\pi}{2}\right). \tag{2}$$

Here, A gives the magnitude of the bias, the excitation level is assumed to be such that $b\tau = n\pi/2$ for $n = 1, 3, 5, 7\ldots$, and $\delta f(\frac{\pi}{2})/f$ is the fractional frequency shift at normal optimal microwave amplitude. Given the cloud size and temperature in NIST-F2 as well as other factors such as toss height and aperture size and placement, the effects that scale in this fashion include microwave leakage and microwave lensing. Second-order effects in the leakage shift leading to quadratic behaviour can, under some circumstances, be as large (or larger) than the first-order effect [35]. In the case of NIST-F2 the state selection cavity has considerably less variation of the tipping angle versus radial position than smaller diameter cavities, and with the cloud sizes, atom temperatures and apertures that apply, the frequency shift versus microwave amplitude is strongly dominated by effects described by equation (2) above. When we fit the data in figure 6 (corrected for other effects, e.g. $m = 0$ DCPS) to the shift given by equation (2) we determine the shift at normal operational power $\left(\frac{\pi}{2}\right)$ to be

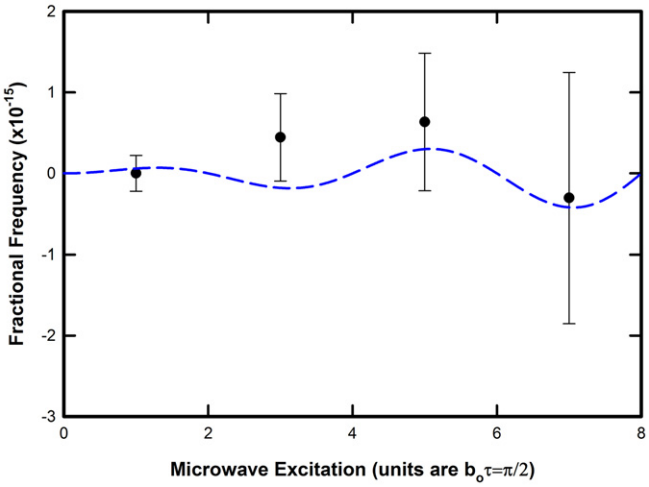

Figure 6. Fractional frequency shift of NIST-F2 as a function of Ramsey microwave amplitude. The dotted line is a fit to equation (2) with an amplitude given by the uncertainty in the fit.

$\delta f/f = (-0.006 \pm 0.08) \times 10^{-15}$; the dotted line in figure 6 is the fitted shift with an amplitude given by the uncertainty in the fit (that is, the dotted line is $\delta f/f = 0.08n\sin(n\pi/2)$, if we plot using the amplitude given by the fit above rather than the uncertainty, it looks like a straight line). Other microwave frequency shifts ($m = 0$ DCPS for example) are evaluated and corrected using theoretically calculated results and called out separately in the uncertainty budget shown in table 1.

3.6. Other frequency biases

3.6.1. First and second-order cavity pulling. The temperature of the NIST-F2 Ramsey cavity changes slightly due to changes in the LN_2 level and the limitations of our liquid fill and temperature-control system. This in turn causes changes in the resonant frequency of the microwave cavity. While cavity pulling in NIST-F1, for example, is considered in the list of uncorrected biases, it is insignificant because it is straightforward to keep the cavity close to resonance such that cavity pulling effects vanish.

The temperature of the NIST-F2 Ramsey cavity is logged every 30 s, and by analysing this record we determine that the cavity is on average detuned 79.4 kHz from resonance. The cavity linewidth is approximately 170 kHz and the temperature tuning coefficient of the cavity is approximately 70 kHz K^{-1}. Furthermore, the cavity temperature varies over about 0.5 K in any 24 h frequency measurement. Any cavity pulling is therefore a dynamic rather than static correction and is not removed during the density extrapolation process.

Using the model developed in [36] and assuming 10^5 detected atoms (a number larger than is ever used in NIST-F2), we estimate any fractional frequency bias due to first-order cavity pulling to be $<10^{-18}$. While the Q of our cavity is high, the density of Cs atoms launched is sufficiently low to make this effect negligible.

Second-order cavity pulling is estimated using the expression found in [37]. The microwave power in NIST-F2 is set within ≈0.3 dBm of optimum power. This gives the magnitude of the bias due to cavity pulling of 1.5×10^{-17}. This bias is uncorrected and we assign the uncertainty to be 100% of the bias.

With slight modifications to the LN_2 control system, it will be possible to reduce the cavity pulling biases by keeping the microwave cavity closer to resonance.

3.6.2. Rabi pulling and Ramsey pulling. Rabi pulling is the result of an underlying baseline slope of the $m = \pm 1$ manifolds. We have measured the fractional $m = \pm 1$ populations after state-selection to be 6×10^{-3}, with a left–right (l–r) asymmetry of 2×10^{-3}, limited by the signal-to-noise ratio of the measurements. Using the analysis in [19], we estimate the bias due to Rabi pulling in NIST-F2 to be negligible and the fractional uncertainty in this bias is $<1 \times 10^{-17}$.

Ramsey pulling in NIST-F2 has been modelled [38] and found to be negligible. The fractional uncertainty due to this bias is $<1 \times 10^{-17}$.

3.6.3. Majorana transitions. In general, in a state-selected fountain where state-selection is performed within the magnetically shielded region, Majorana transitions are possible only after the second Ramsey interaction when the atoms have left the Ramsey interrogation region [2, 39, 40]. In order for a Majorana transition to cause a frequency shift a l–r imbalance (with respect to $|F, 0\rangle$) must be present. In NIST-F2 the required zero in the magnetic field and the required l–r imbalance are both absent. Additionally we use a linearly polarized detection system, thus avoiding the source of l–r asymmetry identified in [40]. We have measured the fractional $m = \pm 1$ populations after state-selection to be 6×10^{-3}, with a l–r asymmetry of 2×10^{-3}, limited by the signal-to-noise ratio of the measurements. Given the conditions of operation of NIST-F2, this leads to a possible fractional bias from Majorana transitions of $\delta f/f < 5 \times 10^{-18}$. We do not correct for this shift.

3.6.4. Resonant light shifts. All resonant laser light sources used for NIST-F2 reside in an adjacent laboratory and the light is delivered to the NIST-F2 via optical fibre cables. Light is attenuated during critical atom-microwave interaction intervals with a two-stage mechanical shutter and electronically by AOMs. Furthermore, light from the AOM is delivered to the physics package by additional fibre optic cables. By measuring the light attenuation factor of each stage and by operating NIST-F2 with various attenuation stages disabled, we estimate any fractional bias due to resonant light to be less than 10^{-18}, with an uncertainty of the same size.

3.6.5. Dc Stark shift. Cs atoms in NIST-F2 are never exposed to insulating surfaces or electrodes with applied voltages, so a bias due to the dc Stark effect is considered unlikely. An insulating area on a surface due to impurities is unlikely, given that the all copper structure was processed in a brazing furnace and standard UHV practices were followed during assembly. The only source of dc voltages is from patch-effect potentials along the microwave cavity and flight tube. Copper surfaces

have varying potentials, but careful measurements [41] have shown they vary on the order of 0.01 V over spatial scales of 10^{-6} m. An unlikely worst-case scenario would be a 0.01 V isolated surface potential as the source of a field 1 cm into the beam tube. This creates a field of only $\approx 1\ \mathrm{V\,m^{-1}}$. If this field were located at apogee it would create a bias of $<10^{-20}$.

3.6.6. Background gas collisions. Vacuum instrumentation (an extended range ionization gauge) near the Cs source chamber in NIST-F2 indicates a pressure $<3 \times 10^{-9}$ Pa. Due to the design of the vacuum system, we expect only background H_2 within the Ramsey region. First, apertures and surfaces between the Cs source chamber and the microwave cavity and time-of-flight tube are fitted with graphite getters to pump background Cs, thus reducing background Cs in the interrogation region. Finally, the cold walls (80 K) of the flight tube cryo-pump many background gases. Using published coefficients for pressure shifts due to H_2 [42, 43] we estimate the fractional frequency shift due to background gases to be $<1 \times 10^{-17}$.

3.6.7. Bloch–Siegert shift. The fractional bias due to the Bloch–Siegert effect in NIST-F2 is estimated using equation 5.6.93(b) in [37] to be 2×10^{-19}, and no correction is made for this effect.

3.6.8. Integrator offset. NIST-F2 uses control software that has been tested for any offsets using several methods as described in [1]. We expect no bias due to integrator offsets and assign a fractional uncertainty of 1×10^{-17}.

4. Results of NIST-F2 accuracy evaluation

The results of nine measurement campaigns of NIST-F2 from September 2010 to August 2013 are shown in figure 7 with respect to TAI. Included in this plot are results from NIST-F1 as well as other primary frequency standards. During this three-year period, improvements were made on NIST-F2 aimed at improving the stability, various control systems including the LN_2 and temperature controls, software used to map the magnetic field, etc. A typical measurement campaign spanned from 10 to 30 days. The fractional frequency difference between NIST-F1 and NIST-F2 during the nine campaigns was $(-0.05 \pm 0.14) \times 10^{-15}$.

5. Conclusion

NIST-F2 is a new primary frequency standard with a cryogenic atom interrogation region that greatly reduces the uncertainty due to the BBR shift. The type A fractional uncertainty for the August 2013 NIST-F2 evaluation was 0.44×10^{-15} and the total type B fractional uncertainty is 0.16×10^{-15}. The type B uncertainty presented in this most recent evaluation is marginally larger than shown in table 1 because the microwave amplitude effects were re-evaluated after the microwave synthesizer was slightly modified. The uncertainty due to the spin-exchange bias is included in the type A uncertainty since it is evaluated using the statistics of the frequency measurements.

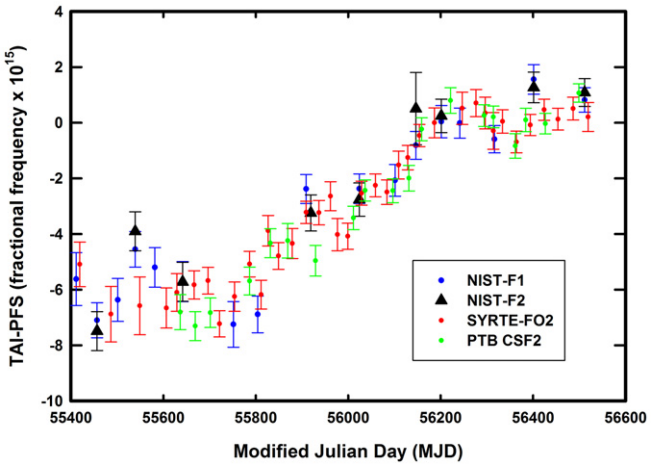

Figure 7. NIST-F2 measurements (black triangles) with respect to TAI from September 2010 to August 2013. For comparison, results from several other primary frequency standards are also shown. The most recent evaluation, August of 2013, is the first NIST-F2 accuracy evaluation submitted to the BIPM. The two NIST measurements on MJD 55539 and MJD 56401 are slightly discrepant with TAI. This is likely a time-transfer problem since NIST-F1 and NIST-F2 showed good in-house agreement.

NIST-F2 will allow for the direct calibration of the BBR bias in the NIST-F1 primary frequency standard in future accuracy evaluations.

Acknowledgments

The authors thank Richard Fox, Tara Fortier, Mike Lombardi, and David Smith for their valuable suggestions and comments that greatly improve this paper.

References

[1] Heavner T P, Jefferts S R, Donley E A, Shirley J H and Parker T E 2005 NIST-F1: recent improvements and accuracy evaluations *Metrologia* **42** 411–22
[2] Jefferts S R *et al* 2002 Accuracy evaluation of NIST-F1 *Metrologia* **39** 321–36
[3] 2012 *BIPM Annual Report on Time Activities* www.bipm.org/utils/en/pdf/time_ann_rep/Time_annual_report_2012.pdf
[4] Wynands R and Weyers S 2005 Atomic fountain clocks *Metrologia* **42** S64–79
[5] Li R, Gibble K and Szymaniec K 2011 Improved accuracy of the NPL-CsF2 primary frequency standard: evaluation of distributed cavity phase and microwave lensing frequency shifts *Metrologia* **48** 283–89
[6] Guéna J *et al* 2012 Progress in atomic fountains at LNE-SYRTE *IEEE Trans. Ultrason. Ferroelectr. Freq. Control* **59** 391–410
[7] Weyers S, Gerginov V, Nemitz N, Li R and Gibble K 2012 Distributed cavity phase frequency shifts of the caesium fountain PTB-CSF2 *Metrologia* **49** 82–7
[8] Heavner T P, Parker T E, Shirley J H and Jefferts S R 2008 NIST F1 and F2 *Proc. 2008 Symp. Frequency Standards and Metrology (Pacific Grove, CA)* pp 299–307
[9] Jefferts S R, Heavner T P, Donley E A, Shirley J and Parker T E 2003 Second generation cesium fountain primary

frequency standards at NIST *Proc. 2003 Joint Meeting IEEE Int. Frequency Control Symp. and EFTF Conf. (Tampa, FL)* pp 1084–88
[10] Donley E A, Heavner T P, O'Brien J W, Jefferts S R and Levi F 2005 Laser cooling and launching performance in a (1,1,1)-geometry atomic fountain *Proc. 2005 Joint Meeting IEEE Int. Frequency Control Symp. and PTTI (Vancouver, Canada)* pp 292–6
[11] Levi F, Calosso C, Calonico D, Lorini L, Costanzo G A, Mongino B, Jefferts S R and Donley E A 2009 The Cryogenic Fountain ITCsF2 *Frequency Control Symp., 2009 Joint with the 22nd European Frequency and Time Forum (Besançon, France)* pp 769–73
[12] Heavner T P, Parker T E, Shirley J H, Donley E A, Jefferts S R, Levi F, Calonico D, Calosso C, Costanzo G and Mongino B 2011 Comparing room temperature and cryogenic cesium fountains *Proc. 2011 Joint Meeting IEEE Int. Frequency Control Symp. and EFTF Conf. (San Francisco, CA)* pp 48–50
[13] Jefferts S R, Drullinger R E and DeMarchi A 1998 Cesium fountain microwave cavities *Proc. 1998 IEEE Int. Frequency Control Symp. (Los Angeles, CA)* pp 6–8
[14] Donley E A, Heavner T P, Levi F, Tataw M O and Jefferts S R 2005 Double-pass acousto-optic modulator system *Rev. Sci. Instrum.* **76** 063122
[15] Heavner T P, Jefferts S R, Donley E A, Parker T E and Levi F 2005 A new microwave synthesis chain for the primary frequency standard NIST-F1 *Proc. 2005 Joint Meeting IEEE Int. Frequency Control Symp. and PTTI (Vancouver, Canada)* pp 308–11
[16] Parker T E, Jefferts S R, Heavner T P and Donley E A 2005 Operation of the NIST-F1 caesium fountain primary frequency standard with a maser ensemble, including the impact of frequency transfer noise *Metrologia* **42** 423–30
[17] Pavlis N K and Weiss M A 2003 The relativistic redshift with 3×10^{-17} uncertainty at NIST, Boulder, CO USA *Metrologia* **40** 66–73
[18] Shirley J H and Jefferts S R 2003 PARCS magnetic field measurement: low frequency Majorana transitions and magnetic field inhomogeneity *Proc. 2003 Joint Meeting IEEE Int. Frequency Control Symp. and EFTF Conf. (Tampa, FL)* pp 1072–5
[19] Shirley J H, Lee W D and Drullinger R E 2001 Accuracy evaluation of the primary frequency standard NIST-7 *Metrologia* **38** 427–58
[20] Leo P J, Julienne P S, Mies F H and Williams C J 2001 Collisional frequency shifts in ^{133}Cs fountain clocks *Phys. Rev. Lett.* **87** 3743–6
[21] Jefferts S R, Heavner T P, Parker T E, Shirley J, Donley E A, Ashby N, Levi F, Calonico D and Costanzo G A 2013 High-accuracy measurement of the blackbody radiation shift of the ground-state hyperfine transition in ^{133}Cs *Phys. Rev. Lett.* **112** 050801
[22] Beloy K, Safronova I and Derevianko A 2006 High-accuracy calculation of the blackbody radiation shift in the ^{133}Cs primary frequency standard *Phys. Rev. Lett.* **97** 040801
[23] Angstmann E J, Dzuba V A and Flambbaum V 2006 Frequency shift of the cesium clock transition due to blackbody radiation *Phys. Rev. Lett.* **97** 040802
[24] Levi F, Shirley J H, Heavner T P, Yu D and Jefferts S R 2006 Power dependence of the frequency bias caused by spurious components in the microwave spectrum in atomic fountains *IEEE Trans. Ultrason. Ferroelectr. Freq. Control* **53** 1584–9
[25] Shirley J H, Levi F, Heavner T P, Calonico D, Yu D and Jefferts S R 2006 Microwave leakage-induced frequency shifts in the primary frequency standards NIST-F1 and IEN-CSF1 *IEEE Trans. Ultrason. Ferroelectr. Freq. Control* **53** 2376–85
[26] Jefferts S R, Shirley J H, Ashby N, Heavner T P, Donley E A and Levi F 2005 On the power dependence of extraneous microwave fields in atomic frequency standards *Proc. 2005 Joint Meeting IEEE Int. Frequency Cont. Symp. and PTTI (Vancouver, Canada)* pp 105–10
[27] Jefferts S R, Shirley J H, Ashby N, Burt E A and Dick G J 2005 Power dependence of distributed cavity phase-induced frequency biases in atomic fountain frequency standards *IEEE Trans. Ultrason. Ferroelectr. Freq. Control* **52** 2314–21
[28] Gibble K 2006 Difference between a photon's momentum and an atom's recoil *Phys. Rev. Lett.* **97** 073002
[29] Ashby N, Barlow S, Heavner T P and Jefferts S R 2014 Frequency shifts in NIST Cs primary frequency standards due to transverse RF field gradients arXiv:1404.4101
[30] Khursheed A, Vecchi G and De Marchi A 1996 Spatial variations of field polarization and phase in microwave cavities: application to the cesium fountain cavity *IEEE Trans. Ultrason. Ferroelectr. Freq. Control.* **43** 201–10
[31] Li R and Gibble K 2004 Phase variations in microwave cavities for atomic clocks *Metrologia* **41** 376–86
[32] Li R and Gibble K 2010 Evaluating and minimizing distributed cavity phase errors in atomic clocks *Metrologia* **47** 534
[33] Guéna J, Li R, Gibble K, Bize S and Clairon A 2011 Evaluation of Doppler shifts to improve the accuracy of primary fountain clocks *Phys. Rev. Lett.* **106** 130801
[34] Santarelli G, Governatori G, Chambon D, Lours M, Rosenbusch P, Guéna J, Chapelet F, Bize S, Tobar M, Laurent P, Portier T and Clairon A 2009 Switching atomic fountain clock microwave interrogation signal and high-resolution phase measurements *IEEE Trans. Ultrason. Ferroelectr. Freq. Control* **56** 1319–26
[35] Weyers S, Schröder R and Wynands R 2006 Effects of microwave leakage in caesium clocks: theoretical and experimental results *Proc. 2006 EFTF (Braunschweig, Germany)* pp 173–80
[36] Bize S, Sortais Y, Mandache C, Clairon A and Salomon C 2001 Cavity frequency pulling in cold atom fountains *IEEE Trans. Instrum. Meas.* **50** 503–6
[37] Vanier J and Audoin C 1989 *The Quantum Physics of Atomic Frequency Standards* (Bristol: Adam Hilger) p 836
[38] Cutler L S, Flory C A, Giffard R P and De Marchi A 1991 Frequency pulling of hyperfine σ transitions in cesium beam atomic frequency standards *J. Appl. Phys.* **69** 2780–92
[39] Bauch A and Schröder R 1993 Frequency shifts in a cesium clock due to Majorana transitions *Ann. Phys., Lpz.* **505** 421–49
[40] Wynands R, Schröder R and Weyers S 2007 Majorana transitions in an atomic fountain clock *IEEE Trans. Instrum. Meas.* **56** 660–3
[41] Witteborn F C and Fairbank W M 1977 Apparatus for measuring the force of gravity on freely falling electrons *Rev. Sci. Instrum.* **48** 1–11
[42] Beer C and Bernheim R 1976 Hyperfine pressure shift of ^{133}Cs atoms in noble and molecular buffer gases *Phys. Rev.* A **13** 1052–7
[43] Happer W 1972 Optical pumping *Rev. Mod. Phys.* **44** 169–250